Journal of Nuclear Materials 442 (2013) S2–S8

Contents lists available at SciVerse ScienceDirect

Journal of Nuclear Materials

journal homepage: www.elsevier.com/locate/jnucmat

Recent progress of R&D activities on reduced activation ferritic/martensitic steels

Q. Huang [a,*], N. Baluc [b], Y. Dai [c], S. Jitsukawa [d], A. Kimura [e], J. Konys [f], R.J. Kurtz [g], R. Lindau [f], T. Muroga [h], G.R. Odette [i], B. Raj [j], R.E. Stoller [k], L. Tan [k], H. Tanigawa [l], A.-A.F. Tavassoli [m], T. Yamamoto [i], F. Wan [n], Y. Wu [a]

[a] Institute of Nuclear Energy Safety Technology, Chinese Academy of Sciences, P.O. Box 1135, Hefei, Anhui 230031, China
[b] CRPP-EPFL, ODGA C110 5232 Villigen PSI, Switzerland
[c] LNM, PSI, 5232 Villigen PSI, Switzerland
[d] JAEA, 2-4 Shirakata, Tokai-Mura, Ibaraki-Ken 319-1195, Japan
[e] IAE, Kyoto University, Gokasho, Uji, Kyoto 611-0011, Japan
[f] KIT, P.O. Box 3640, 76021 Karlsruhe, Germany
[g] PNNL, Richland, WA 99352, USA
[h] NIFS, Oroshi, Toki, Gifu 509-5292, Japan
[i] UCSB, Santa Barbara, CA, USA
[j] IGCAR, Kalpakkam 603 102, India
[k] ORNL, P.O. Box 2008, Oak Ridge, TN 37831, USA
[l] JAEA, Naka, Ibaraki 311-0193, Japan
[m] DMN/Dir, DEN, CEA Saclay, 91191 Gif-sur-Yvette cedex, France
[n] DMPC, USTB, Beijing 100083, China

ARTICLE INFO

Article history:
Available online 3 January 2013

ABSTRACT

Several types of reduced activation ferritic/martensitic (RAFM) steel have been developed over the past 30 years in China, Europe, India, Japan, Russia and the USA for application in ITER test blanket modules (TBMs) and future fusion DEMO and power reactors. The progress has been particularly important during the past few years with evaluation of mechanical properties of these steels before and after irradiation and in contact with different cooling media. This paper presents recent RAFM steel results obtained in ITER partner countries in relation to different TBM and DEMO options.

1. Introduction

Reduced activation ferritic/martensitic (RAFM) steel is considered the reference structural material for future fusion power reactors, due to its technological maturity, i.e. advanced fabrication routes, welding technology and general industrial experience [1,2]. It is also chosen as the main structural material for most ITER test blanket modules (TBMs), which are under development by ITER participants. Hence, RAFM steels are being widely developed in Europe, Japan, Russia, China, the USA and India. Specifically, F82H is being developed by the Japan Atomic Energy Agency (JAEA), JLF-1 by Japanese universities and the National Institute for Fusion Science (NIFS), Eurofer97 is being developed in Europe within the framework of the European Fusion Development Agreement (EFDA) program and Fusion for Energy (F4E) program, China low activation martensitic (CLAM) steel is being developed by the Institute of Nuclear Energy Safety Technology (INEST), Chinese Academy of Sciences (CAS) and 9Cr-2WVTa is being developed by Oak Ridge National Laboratory (ORNL). The specific chemical compositions of the RAFM steels are listed in Table 1 [1–4]. Recent progress has mainly focused on fabrication techniques, mechanical properties, manufacturing of TBMs, the effects of neutron irradiation, compatibility experiments and development of coatings. These are presented in detail in the following sections.

2. Recent progress

2.1. Fabrication of RAFMs

Development of fabrication techniques has mainly focused on purification to reduce neutron-induced activation and on large-scale smelting. The impurities are difficult to control to low levels; they mainly depend on the raw materials and smelting process. The effect of fabrication processes on microstructure and mechanical properties is also being studied.

2.1.1. Production of RAFMs

In 2007, a 5-ton heat of F82H was produced by JAEA using vacuum induction melting (VIM) followed by electro-slag remelting (ESR) [5]. An 11-ton heat of Eurofer97-3 was produced in 2009 fol-

* Corresponding author. Tel.: +86 551 65593328; fax: +86 551 65591397.
E-mail address: qunying.huang@fds.org.cn (Q. Huang).

0022-3115/$ - see front matter © 2012 Elsevier B.V. All rights reserved.
http://dx.doi.org/10.1016/j.jnucmat.2012.12.039

Table 1
Specific chemical compositions of the RAFM steels (wt%).

Element	CLAM	Eurofer97	F82H	JLF-1	9Cr-2WVTa
Fe	Bal.	Bal.	Bal.	Bal.	Bal.
Cr	8.8–9.2	8.5–9.5	7.5–8.5	9.0	8.5–9.0
W	1.3–1.7	1.0–1.2	1.8–2.2	2.0	2.0
V	0.15–0.25	0.15–0.25	0.15–0.25	0.19	0.25
Ta	0.10–0.20	0.10–0.14	0.01–0.06	0.07	0.07
Mn	0.35–0.55	0.20–0.60	0.05–0.20	0.45	0.45
C	0.080–0.12	0.09–0.12	0.08–0.12	0.1	0.1

lowing two other industrial heats, which was melted in a vacuum induction furnace and remelted in a vacuum arc device [6].

In China, a 1.2-ton heat of CLAM steel (HEAT 0912) was prepared by INEST in collaboration with other institutes and companies in China in 2009 with different product forms (bars, plates and tubes) for property testing and studies on fabrication techniques for the TBM [4]. Following on from the combined experience of smelting many small heats- a 4.5-ton batch of CLAM steel (HEAT 1105) was produced with a vacuum induction furnace and vacuum consumable electrode arc furnace in 2011. This was then hot-forged at 1423 K and rolled into different product forms for the fabrication of TBM.

2.1.2. Effect of smelting processes on precipitation behavior

The effect of ESR on the precipitation behavior has been studied [7]. Besides MX particles within the matrix, there were also the rod M_7C_3 carbides and spherical $M_{23}C_6$ carbides existing along lath and grain boundaries in steel melted by VIM. M_7C_3 was precipitated in zones with low W concentration due to macro-segregation of W in the tempered steel, while the rod M_7C_3 carbides were not detected in the steel produced by VIM + ESR due to the improved macro-segregation of W.

2.2. Mechanical properties and microstructure

2.2.1. Precipitation behaviors

Extraction residue analysis was conducted on F82H-BA07 heat, F82H-IEA heat, JLF-1 and CLAM [8]. $M_{23}C_6$ precipitates were coarsened in F82H-BA07 compared with the other steels in the as-normalized and tempered (as-NT) condition, because of the additional normalizing heat treatment. TaC precipitate formation was enhanced in JLF-1 and CLAM compared with F82H-BA07 and F82H-IEA in the as-NT condition, due to the higher Ta content. Laves phase was detected in F82H-IEA after aging above 823 K, where solid-solution W was significantly decreased. However, the amount of solid-solution W is not expected to change after 10,000 h at 873 K and after 1000 h at 923 K. F82H-IEA exhibited hardening after aging at both 673 K and 773 K for 100,000 h, whereas softening occurred at 873 K and 923 K. This behavior is similar to those of JLF-1 and CLAM. Hardening at lower temperatures could be explained by precipitation hardening from TaC, while softening was partly due to loss of solid solution hardening by W.

Precipitation behavior in F82H during blanket fabrication heat treatments, which simulated homogenizing, hot isostatic pressing (HIP) and temperature fluctuations of actual normalizing, was studied by Sakasegawa et al. [9]. Fine particles such as tantalum and vanadium carbides did not precipitate under simulated heat treatments higher than about 1263 K. They should precipitate on packet and block boundaries at lower temperatures such as the tempering temperature.

2.2.2. Fracture toughness

Conventional testing standards used to characterize the fracture resistance of metallic materials always use deeply cracked specimens in order to guarantee high crack tip constraint conditions and small-scale yielding levels. However, structural defects in real components are usually surface cracks that are generated in the course of fabrication. Therefore, predictions of fracture resistance based on standard specimens may be unduly conservative and pessimistic and also can greatly increase the operational and maintenance costs. Hence, the biparameteric fracture behavior with single-edge notched bend (SENB) specimens was assessed by Rodríguez et al. [10]. SENB specimens with shallow cracks always give much higher initiation J values and R-curves with a larger slope than standard deeply cracked specimens. Consequently, accurate failure predictions of real components can only be performed after the calculation of the constraint acting on the component and making use of the J-value characteristic to this particular constraint; otherwise pessimistic expectations would be predicted if the critical J value obtained using standard specimens is used.

2.2.3. Creep properties

Creep-rupture behavior at high temperature is one of the key issues for the application of RAFM steels in a fusion reactor. Fig. 1 shows that F82H has creep strength comparable to that of T91, which is used for high temperature components in power plants worldwide. On the other hand, Eurofer97 showed a bit lower creep strength compared with F82H at higher temperatures, which is probably due to the difference in W concentration [11].

2.2.4. Fatigue properties

In order to develop the fatigue life assessment methods based on the crack growth behavior in RAFM steels, the crack growth behavior under low-cycle fatigue in F82H was investigated by low-cycle fatigue tests at room temperature in air under a total strain in the range of 0.4–1.5% using an hourglass-type miniature fatigue specimen [12]. The relationship between the surface crack length and life fraction was described using one equation independent of the total strain range. Therefore, it might be possible for the fatigue life and residual life of F82H to be predicted using the surface crack length. The microcrack initiation life could be estimated using the total strain range if there is a one-to-one correspondence between the total strain range and the number of cycles to failure. The crack growth rate could be estimated using the total strain range and the surface crack length by introducing the concept of the normalized crack growth rate.

The effect of specimen shape on low-cycle fatigue life of miniature RAFM steels fatigue specimens was studied by Nogami et al. [13]. The differences among the four specimen types tested at relatively high strain ranges (0.8–3.0%) were nearly negligible. The fracture modes of these specimens were almost the same. The stress distribution was independent of the specimen shape above the total strain range of 0.8%, although a significant dependence of the peak stress on the specimen shape was observed under relatively low strain range conditions.

Fatigue life is generally composed of the microcrack initiation stage, crack propagation stage and final fracture stage. Therefore, evaluation of the fatigue behavior of RAFM steels is improved by evaluating not only the overall fatigue life but also the crack growth behavior in the individual stages. The low-cycle fatigue behavior of the miniature fatigue specimens of the RAFM steels was investigated by Nogami et al. [14]. Almost no difference in the microcrack initiation life due to the specimen shape or the total strain range was observed under high strain in the range above 0.8%. Almost no effect of the specimen shape on the normalized crack growth rate was observed under any of the strain range conditions in this work. The normalized crack growth rate was strongly dependent on the total strain range.

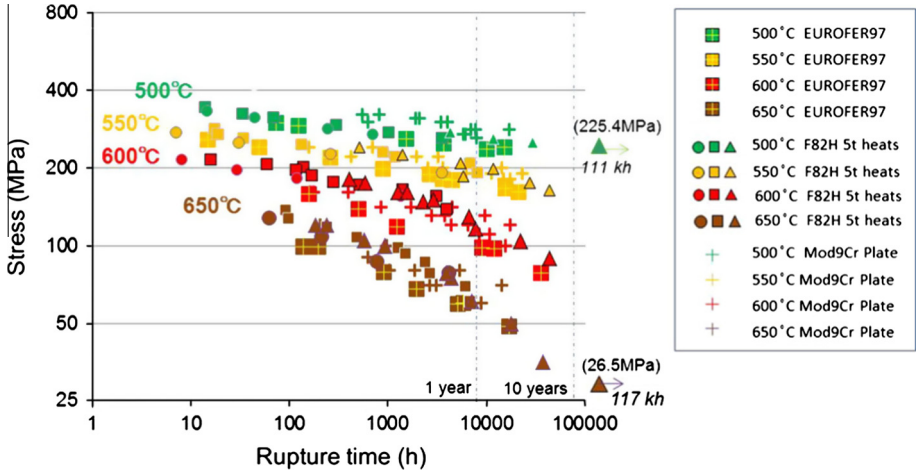

Fig. 1. Creep rupture times of F82H and Eurofer97 at various temperatures.

2.2.5. Thermal aging

Thermal aging is another key factor, which helps to define the design limit of RAFM steels as it is an indication of the phase stability limit. Thermal aging properties of F82H have been previously studied [15]. Laves phase was found at temperatures between 823 K and 923 K after 10,000 h, while M_6C type carbides was found from 773 K to 873 K. These precipitates caused degradation in toughness, especially at temperatures ranging from 823 K to 923 K. Aging didn't affect the tensile properties seriously, except for 923 K aging over 10,000 h, which caused considerable softening to occur. An increase in the precipitates also causes a slight degradation in ductility. A large increase in the ductile-to-brittle transition temperature (DBTT) was observed after 923 K aging. This was caused by large size Laves phase precipitation at the grain boundaries. Laves precipitates at grain boundaries also degrade the upper-shelf energy of aged materials. These aging test results indicated that F82H could be used for up to 30,000 h at 823 K assuming the creep resistance is adequate.

2.3. Effects of irradiation

2.3.1. Irradiation hardening

Irradiation of F82H and Eurofer97 has been carried out in fission reactors under many programs for about 20 years, and it has been reported that irradiation induced hardening appears to saturate between 20 dpa and 70 dpa based on available data [16]. This is supported by some recent data on hardening at high irradiation dose. Latest data from associated reactor irradiation in BOR 60 (ARBOR) for tensile hardening of Eurofer97 and F82H specimens also showed saturation to ~70 dpa at temperatures 573–608 K [16]. A similar hardening and strengthening tendency is evident from indentation and tensile results [17]. Higher discrepancies were seen at higher irradiation temperature, because there was a recovery effect at higher irradiation temperatures that could not be detected in indentations tests performed at room temperature [17]. Post-irradiation annealing of Eurofer97 and other 7–10%Cr-WVTa RAFMs yields substantial recovery of the mechanical properties, indicating recovery of most of the radiation-induced defects [16,18]. The annealing temperature of 773 K was found to be the minimum temperature for starting this recovery [17].

In China, irradiation experiments of CLAM steel started in 2006. In neutron and ion irradiations CLAM steel showed similar results to those of the other RAFMs [19,20]. Recently, some neutron irradiation experiments to more than 20 dpa in domestic and overseas programs were finished, including fission neutron irradiation up to ~1 dpa at 573 K in the high flux engineering test reactor (HFETR) in China, and the spallation neutron irradiation up to ~20 dpa (T_{irr} = 373–773 K) in "SINQ Target Irradiation Program-V" (STIP-V) carried out at the Paul Scherer Institute (PSI) in Switzerland. Post irradiation examination is underway. More specimens of CLAM are being irradiated in STIP-VI to test the mechanical properties and microstructures before and after irradiation in order to investigate the irradiation/helium induced effects [21].

2.3.2. Irradiation embrittlement

Similar to hardening, irradiation induced embrittlement of Eurofer97 and F82H seemed to change slowly with irradiation dose from 20 dpa to 70 dpa at ~603 K, the DBTT shift increased about 25 K [16,22,23]. The Whapham and Makin saturation radiation hardening model [22] worked well for tensile properties. It did not work as well for impact fracture of Eurofer97, but the impact deformation rate was many orders of magnitude higher than that under normal tensile conditions.

Dislocation loops, which exist nearly homogeneously in the Eurofer97 steel matrix, are believed to be the main source of the irradiation hardening and embrittlement [21]. The density of irradiation-induced defects in Eurofer97, which was neutron irradiated to 16.3 dpa, correlated with recent tensile and Charpy results, which showed a maximum irradiation hardening and embrittlement around 573 K [24,25].

In addition, the results of dynamic and static fracture tests of Eurofer97 weld metal were similar, which suggested that there was a low sensitivity of weld metal to neutron irradiation embrittlement in comparison with the base metal.

For the heat treatment effect, tensile and Charpy results indicated that optimization and tightening of the tempering condition improved post-irradiation toughness and ductility. This would be quite beneficial to expand the service condition of RAFMs and give more flexibility for DEMO design [26].

2.3.3. Fatigue after irradiation

Neutron irradiation has only a minor influence on the fatigue accumulation mechanism [16]. When the dose is up to 16.3 dpa (T_{irr} = 523 K), the typical cyclic softening was observed at all strain amplitudes. Furthermore, irradiation to 16–30 dpa at low temperature (523–603 K) was found to be beneficial for low-cycle fatigue life of Eurofer97 at low strain amplitudes, and it was similar with F82H-mod. irradiated to 31 dpa. At high strain amplitudes, the fatigue life was adversely affected because of significant irradiation hardening by dislocation loops, and small α′-precipitates required

a higher stress. A possible explanation for such behavior is that in the low strain range the fatigue damage is postponed by the strong pinning obstacles induced by irradiation, and in the high strain range the fatigue damage built up faster than for the softer material due to localization of deformation [27–29].

2.3.4. Creep under irradiation

Creep under irradiation for F82H and JLF-1 was carried out and evaluated from the diameter change of pressurized tube specimens irradiated to about 5 dpa at temperatures ranging from 573 K to 773 K [30,31]. They exhibited similar irradiation creep behavior up to 5 dpa at 573 K. Creep rupture caused the tubes to fail at stress levels of about 350 MPa and 200 MPa for F82H irradiated to ~5 dpa at 573 K and 773 K, respectively.

2.3.5. Helium effects on hardening

Much attention has been paid to the effect of helium, and helium bubbles where those effects are based on hardening tests and microstructural observations after irradiation in STIP. Preliminary evaluations indicate that the barrier strength (α) of helium bubbles with sizes 1–1.5 nm is 0.1 based on the preliminary evaluations of F82H and Optimax-A. Although the small He bubbles are weak obstacles, significant hardening can still be produced because of their very high density, 10^{23}–10^{24} m^{-3} [32].

Microstructure data after irradiation up to 1500 appm He and 25 dpa from HFIR (High Flux Isotope Reactor) ISHI (In Situ Helium Implantation), showed that small bubbles and larger voids were observed and these were precursors to significant swelling [33].

Microstructure changes induced by electron irradiation have been studied in deuterium-implanted CLAM specimens. The D–I (Defect–Interstitial atoms) and D–Is (Defect–Interstitial atom clusters) complexes would form interstitial loops, D–V (Defect–Vacancies) complexes would cluster to form vacancy loops, and D–Vs (Defect–Vacancy clusters) complexes would cluster to form voids.

2.3.6. Helium effects on embrittlement

A study of the tensile properties and fracture mechanisms of Eurofer97 implanted with H and He was carried out when both species were present. No effect of pre-implanted He or H embrittlement was observed, neither when He was in the as-implanted condition, nor when bubbles had been formed [34]. To investigate extra He effects, irradiation data from ^{10}B-doped Eurofer97 specimens showed embrittlement and reduction of toughness with an increased He amount [16,35]. From microstructure observations, very few and completely non-homogeneously distributed voids or He bubbles were found. This was attributed to the production of He from segregated boron [23].

2.4. Compatibility experiments

Liquid PbLi alloy is one of the candidate materials for coolants and breeders in fusion reactors due to its favorable breeder and coolant properties [36,37]. However, corrosion of candidate structural materials presents a critical challenge in the use of liquid PbLi alloy in fusion reactors, as it can affect the properties of structural materials due to changes in the microstructure, composition and surface morphology [35,36,38,39].

The relative resistance of various RAFMs to liquid PbLi corrosion was tested in PbLi loops and small devices at different temperatures and flow rates related to the different blanket PbLi concepts in the world.

Moreau et al. [40] investigated Eurofer97 corrosion and dissolution properties associated with MHD (magnetohydrodynamics) flow present in near-wall regions in liquid PbLi. A model was developed that was based on a thermodynamic analysis of the dissolution and electrodissolution mechanisms, which were introduced to explain this phenomenon. Chen et al. [41] performed corrosion tests for CLAM specimens in the thermal convection liquid PbLi loop DRAGON-I at 753 K with a flow velocity of 0.08 m/s for more than 8000 h (see Fig. 2). The corrosion rate of CLAM specimens was ~17 μm/year under such conditions.

Kondo et al. [42] found that JLF-1 suffered corrosion attack non-uniformly to some boundaries of the microstructure caused by peeling of sub-grains after corrosion on the specimen surface. A mass transfer model was also used to evaluate the mass loss of the materials exposed to PbLi. It showed that the experimental data agreed with the results of the mass transfer model.

Konys et al. [43] studied the corrosion behavior of Eurofer97 in compatibility tests at a flow rate of 0.22 m/s and 0.10 m/s in the forced convection non-isothermal liquid PbLi loop PICOLO and obtained many results at temperatures up to 823 K. The dissolution rates were ~400 μm/yr and ~250 μm/yr, respectively. Meanwhile, modeling tools to describe the corrosion rate and to extrapolate to DEMO conditions have been developed and integrated in the oxidation and mass transfer calculation code MATLIM at the Karlsruhe Institute of Technology (KIT). The simulated corrosion data was consistent with the experimental results obtained earlier at 0.22 m/s at 753 K and 823 K (see Fig. 3).

2.5. Development of coatings

Tritium permeation and leakage, corrosion and MHD effects, etc. are key issues of liquid breeder blankets with RAFMs. Coatings on RAFM steels are one of the solutions to these issues. On the basis of long-term candidate materials screening, current R&D activities on coatings are mainly focused on Al_2O_3 and Er_2O_3 coatings.

Various methods have been used to fabricate Al_2O_3 coatings, but most of the technologies were not suitable for a realistic blanket geometry. However, some other chemical processes showed some flexibility to coat complex geometries, such as sol–gel methods. Ueki et al. [44] investigated the electrical insulation of Al_2O_3 coating fabricated by sol–gel method in PbLi. The results showed that the coating had the potential to work as an electrical insulation coating for a PbLi blanket. However, the operation time and the temperature should be limited since the electrical insulation breaks above 673 K. This electrical insulation failure was not from the PbLi corrosion but due to the mismatch between the thermal expansions of the sol–gel coating and the substrate. Further studies on fabrication process and coating performance are necessary, especially on their attachment and cracking of the coating formed by the sol–gel method.

Early results from the hot-dip aluminization (HDA) process study suggested that an Al-based coating had the potential to work as a corrosion and tritium permeation barrier [45,46], but HDA had great difficulty in controlling the thickness of the Al scale and removing excessive Al. A recently developed Al-electroplating technique provided a better way to fabricate excellent aluminum coatings on steels with controllable thickness, in contrast to HDA.

Corrosion resistance is an essential requirement of coatings. In preliminary service performance testing, the Al-based coatings fabricated by the electrochemical deposition method have shown excellent corrosion resistance to PbLi [47]. There is no report on the results of permeation resistance testing of Al-based coatings on RAFMs yet, but Zhang's results [48] showed that Al-based coatings on HR-2 steel prepared by a similar process reduced the deuterium permeation by two to three orders of magnitude in the gas phase at 873–1000 K. All these results suggest that the Al-electroplating process might be an appropriate method for applying Al-based coatings to blanket components.

Al-pack cementation is another Al-based coating fabrication method. Yang et al. [49] developed a specific pack-cementation method to fabricate Al_2O_3 coatings. The specimens were coated

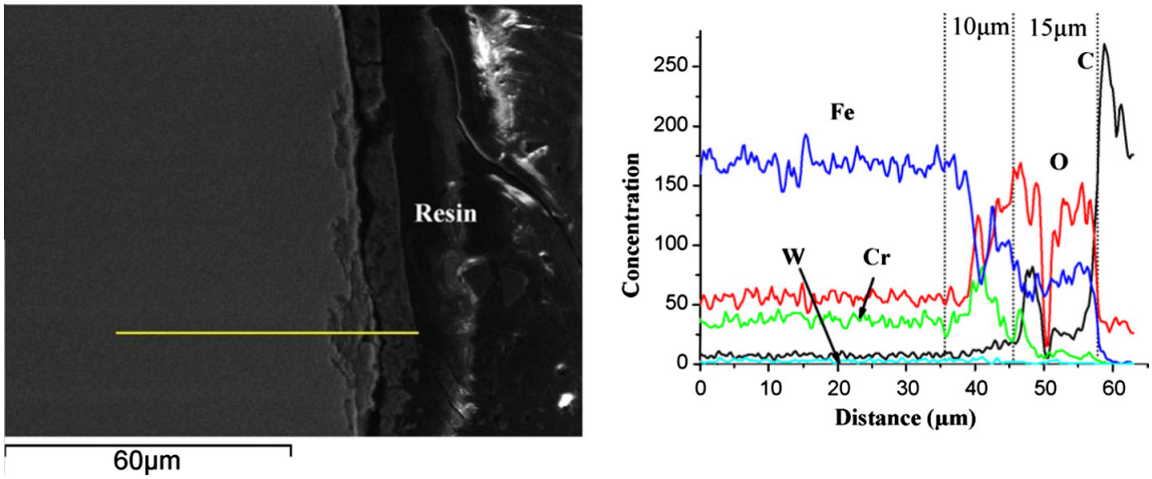

Fig. 2. Cross-section line analysis of CLAM specimen after 8000 h of exposure at 753 K.

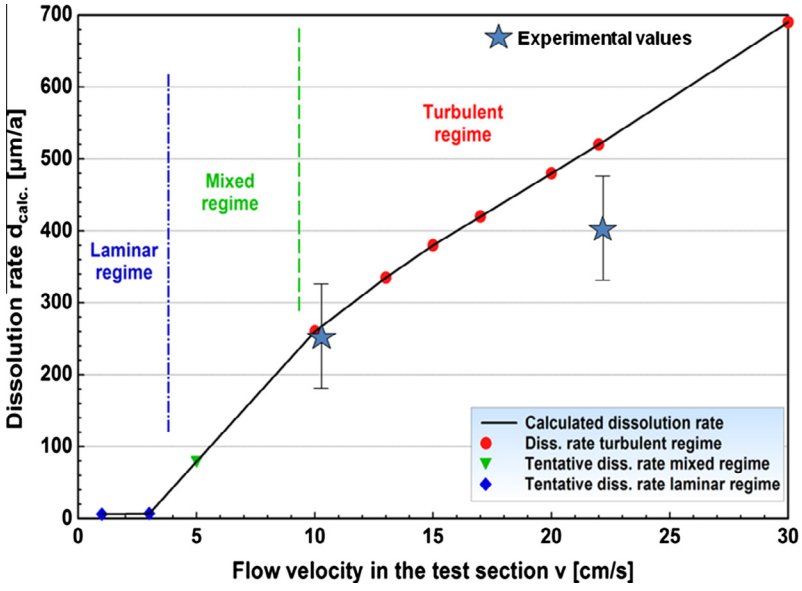

Fig. 3. Corrosion behavior of Eurofer97.

with Al layer by low-activity pack-aluminizing and then grew Al_2O_3 on the surface by in situ oxidation. Current research results show that the coating produced by this method on 316L tubular specimens achieved a tritium permeation reduction factor of more than 3000 in gas-phase tests.

An Er_2O_3 coating is regarded as one of the candidate MHD coatings for Li and PbLi breeder blankets due to its good compatibility and electrical insulation even under irradiation [50,51]. The tritium-permeation reduction ability of Er_2O_3 coating on steels by sol–gel method [52] and filtered arc deposition [53] was demonstrated. Recently the feasibility with metal–organic decomposition was also explored [54]. Further study on in situ growth in liquid PbLi and its application to PbLi blankets is necessary.

2.6. Fabrication techniques of TBM by RAFMs

The fabrication of TBM with RAFM steel mainly includes the manufacture of the first wall (FW), the cooling plates (CPs) and the assembly of these subcomponents. HIP diffusion welding (HIP-DW) is considered as a promising technology to fabricate the components with complex cooling channels for the ITER-TBM due to its advantages associated with non-melting [55]. Also, electron beam (EB) welding, tungsten inert gas (TIG) welding, and laser welding are candidate welding techniques for the assembly of the subcomponents of TBM.

2.6.1. Fabrication techniques for the FW

A lot of research on HIP-DW of the RAFMs has been done in the world. The subcomponents with internal cooling channels are obtained by diffusion bonding processes. Among the envisaged techniques, the three most promising ones are as follows:

(i) The "improved two-step HIP" process: a first HIP cycle at low pressure is used to seal the plates without significant deformation of the channels; a second high pressure HIP cycle is then applied to the structure with counter pressure inside the channels to avoid collapse. This process has been shown to require special attention with respect to fabrication procedure to avoid the formation of oxides at the joints, which degrade the impact toughness [56].

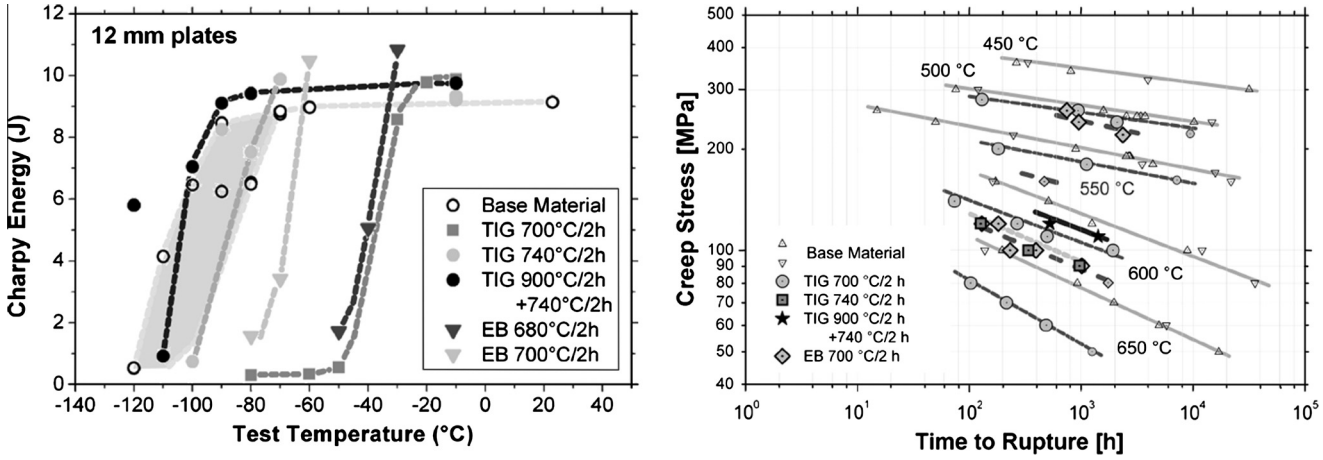

Fig. 4. Charpy and creep test results of 12 mm EB and TIG welds of Eurofer97 with different PWHTs.

(ii) The "tubes forming + HIP" technique has two kinds of processes. One is to use thin tubes inserted between the grooved plates before HIPing of the whole assembly; during a HIP cycle, the thin tubes expand and conform to the rectangular grooves. The other is to use the relatively thick rectangular tube and two plates [57]. These processes should focus on the U-shape rectangular tubes forming for the FW fabrication.

(iii) The "weld + HIP" process consists of welding thin strips on the top of each groove and then adding a plate by HIP. Previous optimizations have resulted in the fabrication and the thermomechanical test of a CP test mock-up featuring straight internal channels. The development of this process has been pursued focusing on welding procedures for bent channels and the sensitivity to the positioning of the welded joint.

(iv) Several HIP experiments on CLAM have been performed and good joints were obtained through the optimization of HIP conditions. The tensile properties of HIP joints are identical to those of the base metal. The absorbed impact energy of some joints reached the level of the base metal [58].

2.6.2. Fabrication techniques for rectangular tubes for the FW

In order to achieve better cooling and easy installation, the FW cooling channels of the dual-cooled liquid metal blanket designs carried out in the world are mainly focusing on a rectangular style.

Hirose et al. [59] successfully fabricated an F82H steel rectangular tube through drawing work, and the length of the rectangular tube is suitable for the fabrication of the FW. The Eurofer97 steel rectangular tube is made by hydroforming after annealing, but with a large fillet radius.

The CLAM steel round tube was made through hot piercing, reducing diameter by cold-drawing and the rectangular tube was made by cold-rolling work with a fillet radius. Also thin U-shape rectangular tubes are being fabricated by hydrofroming techniques [60].

2.6.3. Fusion welding techniques for assembling the subcomponents

The complicated structure of TBM makes the assembly of the components difficult. According to the current designs for TBMs, some subcomponents have to be assembled: FW, caps, back plates, and so on. Assembly of the key components by fusion welding techniques, such as TIG, NGTIG (narrow gap tungsten inert gas), fiber laser, laser/MIG (metal inert gas) hybrid and EB, is being developed. Some of these processes need to be modeled and optimized with simulations.

Fig. 4 [61] shows some Charpy and creep test results of 12 mm EB and TIG welds of Eurofer97 with different post-weld heat treatments (PWHTs).

The properties and microstructures of the welded joints of RAFMs, such as F82H, are being widely investigated [11]. The results show there are no significant technical issues for welded joints of RAFMs. Some irradiation tests of welded joints have been done, but PWHT may be optimized further to improve residual stress, mechanical properties and irradiation effects.

Several components of the Eurofer97 mock-ups have been laser welded, including a "one cell mock-up", using strong internal and external clamping tools. It can be concluded that distortions in the TBM can be managed using high-power laser and laser/MAG (metal active gas) hybrid welding and industry can easily adapt the procedures specified here for TBM manufacturing. The welder qualification and certification required for these processes is not more demanding than that needed for Manual TIG and NGTIG processes [62].

In addition, development of the assembly process for the TBM is being performed in China by fabricating a one-third-scale TBM mockup with T91 [4]. Furthermore, a one-third-scale TBM mockup of CLAM steel will also be fabricated in China based on the previous experience.

Although mockups of the TBMs have been fabricated, more efforts on the fabrication techniques of TBM are still needed, e.g. the inspection of diffusion welds for components with flow channels, the welding of difficult-to-reach positions and the development of tritium permeation barriers.

3. Summary

Great progress has been made on RAFM steel development, e.g. large-scale fabrication, mechanical properties testing before and after neutron irradiation, fabrication of TBM, etc. For applications in DEMO and fusion reactors, more efforts are still needed in the following aspects:

(1) Studies on the helium and hydrogen synergetic effect with displacement damage and the effects of other transmutation products on properties of RAFMs, especially by using IFMIF (International fusion Materials Irradiation Facility) or small fusion reactors in the future.

(2) Development of inspection methods of diffusion welds for TBM components with flow channels, welding techniques for difficult-to-reach positions, and fabrication of tritium permeation barriers.

Acknowledgement

Thanks to all the other colleagues for their hard work and good progress on R&D of RAFMs to push its final application.

Reference

[1] N. Baluc, K. Abe, J.L. Boutard, V.M. Chernov, E. Diegele, S. Jitsukawa, et al., Nucl. Fusion 47 (2007) S696–S717.
[2] R.J. Kurtz, A. Alamo, E. Lucon, Q. Huang, S. Jitsukawa, A. Kimura, et al., J. Nucl. Mater. 386–388 (2009) 411–417.
[3] W. Bahm, Materials development – structural materials, nuclear fusion programme annual report of the association Forschungszentrum Karlsruhe/EURATOM, Forschungszentrum Karlsruhe GmbH, Karlsruhe, FZKA 7117, 2005.
[4] Q. Huang, Q. Wu, S. Liu, C. Li, B. Huang, L. Peng, et al., Fusion Eng. Des. 86 (2011) 2611–2615.
[5] T. Nishitani, H. Tanigawa, S. Jitsukawa, T. Nozawa, K. Hayashi, T. Yamanishi, et al., J. Nucl. Mater. 386–388 (2009) 405–410.
[6] Y. Poitevin, The tritium breeding blankets for fusion reactors – a key component for sustainability of fusion energy, Swiss Nuclear Forum, CRPP/Lausanne, March 23, 2011.
[7] Z. Xia, C. Zhang, H. Lan, Z. Yang, P. Wang, J. Chen, et al., Mater. Sci. Eng. A 528 (2010) 657–662.
[8] T. Nagasaka, Y. Hishinuma, T. Muroga, Y. Li, H. Watanabe, H. Tanigawa, et al., Fusion Eng. Des. 86 (2011) 2581–2584.
[9] H. Sakasegawa, H. Tanigawa, S. Kano, M. Enomoto, Fusion Eng. Des. 86 (2011) 2541–2544.
[10] C. Rodríguez, F.J. Belzunce, T.E. García, I. Peñuelas, Procedia Eng. 10 (2011) 977–982.
[11] H. Tanigawa, K. Shiba, A. Möslang, R.E. Stoller, R. Lindau, M.A. Sokolov, et al., J. Nucl. Mater. 417 (2011) 9–15.
[12] S. Nogami, Y. Sato, A. Hasegawa, J. Nucl. Sci. Technol. 47 (2010) 457–461.
[13] S. Nogami, Y. Sato, A. Tanaka, A. Hasegawa, A. Nishimura, H. Tanigawa, J. Nucl. Sci. Technol. 47 (2010) 47–52.
[14] S. Nogami, Y. Sato, A. Hasegawa, H. Tanigawa, M. Yamazaki, M. Narui, J. Nucl. Mater. 417 (2011) 131–134.
[15] K. Shiba, H. Tanigawa, T. Hirose, H. Sakasegawa, S. Jitsukawa, Fusion Eng. Des. 86 (2011) 2895–2899.
[16] E. Gaganidze, C. Petersen, E. Materna-Morris, C. Dethloff, O.J. Weiß, J. Aktaa, et al., J. Nucl. Mater. 417 (2011) 93–98.
[17] I. Sacksteder, H.-C. Schneider, E. Materna-Morris, J. Nucl. Mater. 417 (2011) 127–130.
[18] E. Materna-Morris, A. Möslang, R. Rolli, H.-C. Schneider, J. Nucl. Mater. 386–388 (2009) 422–425.
[19] L. Peng, Q. Huang, C. Li, S. Liu, J. Nucl. Mater. 386–388 (2009) 312–314.
[20] Q. Huang, Y. Wu, J. Li, F. Wan, J. Chen, G. Luo, J. Nucl. Mater. 386–388 (2009) 400–404.
[21] Y. Dai, L. Zanini, N. Baluc, G.R. Odette, Utilizing the Swiss spallation neutron source for fusion materials research, Presented at ICFRM-15, Charleston, South Carolina, October 16–22, 2011.
[22] Bob van der Schaaf, C. Petersen, Y. De Carlan, J.W. Rensman, E. Gaganidze, X. Averty, J. Nucl. Mater. 386-388 (2009) 236–240.
[23] J. Henry, X. Averty, A. Alamo, J. Nucl. Mater. 417 (2011) 99–103.
[24] M. Klimenkov, E. Materna-Morris, A. Möslang, J. Nucl. Mater. 417 (2011) 124–126.
[25] E. Lucon, W. Vandermeulen, J. Nucl. Mater. 386–388 (2009) 254–256.
[26] K. Shiba, E. Wakai, T. Sawai, M. Ando, H. Tanigawa, T. Hirose, et al., Irradiation effects on deformation and fracture of reduced activation ferritic steels, Presented at ICFRM-15, Charleston, South Carolina, USA, October 16–22, 2011.
[27] E. Materna-Morris, A. Möslang, R. Rolli, H.-C. Schneider, Fusion Eng. Des. 86 (2011) 2607–2610.
[28] C. Petersen, A. Povstyanko, V. Prokhorov, A. Fedoseev, O. Makarov, M. Walter, et al., J. Nucl. Mater. 386–388 (2009) 299–302.
[29] N.V. Luzginova, J. Rensman, P. ten Pierick, J.B.J. Hegeman, J. Nucl. Mater. 409 (2011) 153–155.
[30] N. Okubo, K. Shiba, M. Ando, T. Hirose, H. Tanigawa, E. Wakai, et al., Reduced activation ferritic/martensitic steel F82H for in-vessel components – improvement of irradiation response of toughness and ductility, Presented at ICFRM-15, Charleston, South Carolina, USA, October 16–22, 2011.
[31] M. Ando, M. Li, M. L. Grossbeck, L. T. Gibson, H. Tanigawa, K. Shiba, et al., Creep behavior of RAFM irradiated at 300 and 500 °C up to 5 dpa, Presented at ICFRM-15, Charleston, South Carolina, USA, October 16–22, 2011.
[32] L. Peng, Y. Dai, J. Nucl. Mater. 417 (2011) 996–1000.
[33] G. R. Odette, T. Yamamoto, N. Cunningham, E. Stergar, D. Edwards, The effects of helium on cavity evolution in tempered martensitic steels and nanostructured ferritic alloys – in situ helium implantation studies, Presented at ICFRM-15, Charleston, South Carolina, USA, October 16–22, 2011.
[34] P. Jung, H. Klein, J. Henry, J. Chen, J. Nucl. Mater. 417 (2011) 1013–1017.
[35] E. Gaganidze, C. Petersen, J. Aktaa, J. Nucl. Mater. 386–388 (2009) 349–352.
[36] H. Moriyama, A. Sagara, S. Tanaka, R.W. Moir, D.K. Sze, Fusion Eng. Des. 39–40 (1998) 627–637.
[37] L. Giancarli, V. Chuyanov, M. Abdou, M. Akiba, B. Hong, R. Lässer, et al., J. Nucl. Mater. 367–370 (2007) 1271–1280.
[38] D. Petti, G. Smolik, M. Simpson, J. Sharpe, R. Anderl, S. Fukada, et al., Fusion Eng. Des. 81 (2006) 1439–1449.
[39] T. Muroga, M. Gasparotto, S.J. Zinkle, Fusion Eng. Des. 61–62 (2002) 13.
[40] R. Moreau, Y. Bréchet, L. Maniguet, Fusion Eng. Des. 86 (2011) 106–120.
[41] Y. Chen, Q. Huang, S. Gao, Z. Zhu, X. Ling, Y. Song, et al., Fusion Eng. Des. 85 (2010) 1909–1912.
[42] M. Kondo, T. Muroga, A. Sagara, T. Valentyn, A. Suzuki, T. Terai, et al., Fusion Eng. Des. 86 (2011) 2500–2503.
[43] J. Konys, W. Krauss, H. Steiner, J. Novotny, A. Skrypnik, J. Nucl. Mater. 417 (2011) 1191–1194.
[44] Y. Ueki, T. Kunugi, N.B. Morley, M.A. Abdou, Fusion Eng. Des. 85 (2010) 1824–1828.
[45] J. Konys, W. Krauss, Z. Voss, O. Wedemeyer, J. Nucl. Mater. 367–370 (2007) 1144–1149.
[46] A. Aiello, J. Nucl. Mater. 329–333 (2004) 1398–1402.
[47] J. Konys, W. Krauss, N. Holstein, Fusion Eng. Des. 85 (2010) 2141–2145.
[48] G. Zhang, J. Li, C. Chen, S. Dou, G. Ling, J. Nucl. Mater. 417 (2011) 1245–1248.
[49] H. Yang, Q. Zhan, W. Zhao, X. Yuan, Y. Hu, Z. Han, J. Nucl. Mater. 417 (2011) 1237–1240.
[50] T. Shikama, R. Knitter, J. Konys, T. Muroga, K. Tsuchiya, A. Moesslang, et al., Fusion Eng. Des. 83 (2008) 976–982.
[51] T. Tanaka, B. Tsuchiya, F. Sato, T. Shikama, T. Iida, T. Muroga, Fusion Eng. Des. 83 (2008) 1300–1303.
[52] Z. Yao, A. Suzuki, D. Levchuk, T. Chikada, T. Tanaka, T. Muroga, et al., J. Nucl. Mater. 386–388 (2009) 700–702.
[53] T. Chikada, A. Suzuki, Z. Yao, D. Levchuk, H. Maier, T. Terai, et al., Fusion Eng. Des. 84 (2009) 590–592.
[54] T. Chikada, A. Suzuki, T. Tanaka, T. Terai, T. Muroga, Fusion Eng. Des. 85 (2010) 1537–1541.
[55] K. Furuya, E. Wakai, M. Ando, T. Sawai, A. Iwabuchi, K. Nakamura, et al., Fusion Eng. Des. 69 (2003) 385–389.
[56] M. Rieth, A Cost-effective, Large-scale and Fail-safe First Wall Fabrication Method, Portland, Oregon, USA, September 11–16, 2011.
[57] H. Tanigawa, H. Tanigawa, T. Hirose, M. Enoeda, H. Serizawa, Y. Kawahito, Manufacturing technology of F82H for application to test blanket module, Presented at ICFRM-15, Charleston, South Carolina, USA, October 16–22, 2011.
[58] C. Li, Q. Huang, Q. Wu, S. Liu, Y. Lei, T. Muroga, et al., Fusion Eng. Des. 84 (2009) 1184–1187.
[59] T. Hirose, H. Tanigawa, M. Enoeda, M. Akiba, Fusion Sci. Technol. 52 (2007) 839–843.
[60] B. Huang, Q. Huang, C. Li, S. Liu, Q. Wu, Fusion Eng. Des. 86 (2011) 2602–2606.
[61] M. Rieth, J. Rey, J. Nucl. Mater. 386–388 (2009) 471–474.
[62] P. Aubert, F. Tavassoli, M. Rieth, E. Diegele, Y. Poitevin, J. Nucl. Mater. 417 (2011) 43–50.